Applied Surface Science 563 (2021) 150392

Contents lists available at ScienceDirect

Applied Surface Science

journal homepage: www.elsevier.com/locate/apsusc

Full Length Article

Improved contact properties of graphene-metal hybrid interfaces by grain boundaries

Junfei Ding [a], Qiushi Yao [c], Huasheng Sun [a], Shanbao Chen [a], Ting Hu [a,b,*], Erjun Kan [a,b,*]

[a] Department of Applied Physics and Institution of Energy and Microstructure, Nanjing University of Science and Technology, Nanjing, Jiangsu 210094, PR China
[b] Key Laboratory of Soft Chemistry and Functional Materials, Nanjing University of Science and Technology, Nanjing, Jiangsu 210094, PR China
[c] Department of Physics, Southern University of Science and Technology, Shenzhen, 518055 Guangdong, PR China

ARTICLE INFO

Keywords:
Two-dimensional materials
Graphene-metal contacts
Grain boundaries
Interface barrier
Density functional theory
Transition-Metal surfaces

ABSTRACT

Graphene-metal (MGr) hybrid contacts have been broadly used to improve the contact properties of two-dimensional (2D) electric devices. Since grain boundaries of graphene are inevitable, it is quite necessary to investigate how the grain boundaries affect the contact properties of graphene-metal interfaces. Herein, based on first-principles calculations, we comprehensively studied the contact properties of graphene with grain boundaries deposited on different transition metals substrates including Ni, Pd and Cu(1 1 1) slabs. Our calculations show that the grain boundaries always narrow and lower the tunneling barrier of the contacts, which will significantly increase the tunneling possibility of the carriers at the contacts. These results suggest a very convenient method to improve the performance of the graphene-based devices.

1. Introduction

Over the past decade, two-dimensional materials, especially van der Waals layered materials [1,2], have been widely used as the channel (such as MoS_2), dielectric (h-BN) and contacts materials in the field-effect-transistor based devices [3], due to their many unique characteristics not found in their bulk counterparts [4]. However, the large contact resistance (R_c) between the contacts and the channel limits the ultimate performance [5]. For example, the typical value of R_c between metal and monolayer transition-metal dichalcogenides (mTMDs) is usually 1–3 orders higher [6,7] than that of metal-silicon contacts in complementary metal oxide semiconductor technology (order of 0.1 $k\Omega\cdot\mu m$) [8] and such high metal-mTMDs contact resistances significantly degrade the performance of TMD transistors [9].

Among many methods suggested to improve the contact properties (such as vacancies [10], self-assembly [11], phase engineering [7] and one dimensional edge contacts [12]), metal-graphene hybrid contact [13–15] is an efficient strategy to reduce the contact resistance of two dimensional material based field effect transistors. Therefore, it is crucial to study the contact properties at the metal-graphene interface [15] and explore the strategies to reduce the contact resistance.

It is known that grain boundaries are always inevitable in typical graphene grown by chemical vapor deposition [16,17] on metal foils. However, atomic understanding of the contacts with grain boundaries is still absent. Therefore, it is important to explore how the grain boundaries affect the contact resistance.

According to the binding strength of the graphene-metal (MGr) interfaces explored by previous studies [18–21], graphene monolayer absorbed on metal substrates can be divide into two classes [18]: 1) chemisorption on Co, Ni, and Pd(1 1 1) which leads to a strong bonding and 2) physisorption on Al, Cu, Ag, Au, and Pt(1 1 1) which leads to a weaker bonding. Herein, we choose Ni, Pd and Cu(1 1 1) contacts, which stand for the strong, intermediate and weak bonding situations respectively, to explore the impact of grain boundaries in metal-Gr hybrid contacts. Adopting the coincidence lattice theory [22,23], different types of grain boundaries (whether consist of 4–8 rings or 5–7 rings) in graphene can be constructed by tuning the misorientation angle (θ), however, limited by computing resource, we only construct the type of grain boundary of graphene with $\theta = 21.8^{\circ}$, which contain relatively less atoms in a supercell comparing to the other types of grain boundaries and also observed in experiment [24,25]. According to the elasticity theory [23], the interaction between grain boundaries decays exponentially with the separate distance, and here, we have inserted 4 six-membered C rings between two boundaries to reduce this interaction,

* Corresponding authors at: Department of Applied Physics and Institution of Energy and Microstructure, Nanjing University of Science and Technology, Nanjing, Jiangsu 210094, PR China.
E-mail addresses: thu@njust.edu.cn (T. Hu), ekan@njust.edu.cn (E. Kan).

https://doi.org/10.1016/j.apsusc.2021.150392
Received 17 January 2021; Received in revised form 10 May 2021; Accepted 13 June 2021
Available online 17 June 2021

which is long enough to buffer the interaction between grain boundaries. For convenience, we use 21.8-Gr, 21.8-MGr (M = Ni, Pd, Cu) to denote the graphene monolayer and metal-graphene contact with grain boundaries structures, respectively.

Our results show that grain boundaries always enhance the interaction between graphene and metals, and the 5–7 rings in graphene are bent toward the metal surface which buckle the graphene monolayer. While for the contact properties, we found that the tunneling barrier has disappeared both in NiGr and 21.8-NiGr contacts due to the strong interaction between graphene and Ni. For the Cu and Pd cases, the tunneling barrier is narrowed and lowered by grain boundaries, especially for the PdGr contact, the tunneling possibility is largely increased from 13.63% in PdGr to 50.12% in 21.8-PdGr contacts. Thus, our results indicate that the grain boundaries will lower the contact resistance by increasing the tunneling possibility in all graphene-metal hybrid contacts.

2. Computational details and methods of analysis

Our first-principles calculations are based on density functional theory (DFT) with generalized gradient approximation (GGA) for exchange correlation potential given by Perdew-Burke-Ernzerhof (PBE) [26], as implemented in the Vienna Ab initio Simulation Package (VASP) [27]. A van der Waals (vdW) correction proposed by Grimme (DFT-D2) [28] was chosen due to its good description of long-range vdW interactions [29,30]. The projected augmented wave (PAW) method with a plane-wave basis set was used [31,32]. We set the energy cutoff and convergence criteria for energy and force to be 500 eV, 10^{-4}eV, and 0.01 eVÅ^{-1}, respectively. Dipole correction [33,34] is used to calculate the electrostatic potential of the interfaces. The PHONOPY package [35] is adopted to calculate the phonon dispersion of 21.8-Gr monolayer and its thermal stability is confirmed by ab Initio Molecular Dynamics (AIMD) simulations.

The surface calculations have been performed within slab model, involving three metal layers with atoms in the bottom two layers fixed to their bulk positions. Repeated slabs were separated by more than 15 Å to avoid interaction between each other. During the MGr contacts calculation, for NiGr and CuGr, 1 × 1 commensurate structure is used, while for PdGr, $\sqrt{3} \times \sqrt{3}$ Pd is used to match the 2 × 2 supercell of graphene (Fig. 1 in supplementary material shown the stable structures of MGr interfaces). The lattice mismatch of CuGr, NiGr, and PdGr are 3.70%, 0.42% and 1.81%, respectively. For the 2-dimensional materials, any change to the lattice constant may affect the materials' properties, considering this point, many literatures [36] have adopted the strategy that matching the lattice of metal to graphene's if the mismatch is in the reasonable range. And in this study, we also employed this approach to avoid the introduction of stress in graphene as much as possible. 8 × 2 × 1 and 14 × 2 × 1 K-point are adopted for the optimization and total energy calculations of the structures with grain boundaries, respectively.

3. Results

For the 21.8-graphene monolayer, grain boundaries are marked by shadows in Fig. 1**b**, which consist of repeating 5–7 ring pairs with a single intermediate hex-rings. As shown in Fig. 1**a**, the structure is slightly buckled with 0.145 Å. The calculated phonon dispersion and variation of the total potential energy of 21.8-Gr with simulation time during AIMD simulation are displayed in Fig. 1**c and 1d**, respectively. As shown in Fig. 1a, there are no imaginary modes in the entire Brillouin zone, which demonstrates that the 21.8-Gr is dynamically stable. And the average values of the total potential energy remain nearly constants during the entire simulations, confirming that 21.8-Gr is thermally stable at 300 K. In Fig. 1**e and 1f** we also display the band structures of graphene and 21.8-graphene monolayer, respectively, and the calculated energy gap of 21.8-graphene is 45 meV, which indicates the effect of grain boundaries.

The structure configurations of metal-graphene interfaces without grain boundaries are displayed in Fig. 1**s** in supplementary material. In the cases of Ni and Cu, the adsorption positions of graphene on Cu and

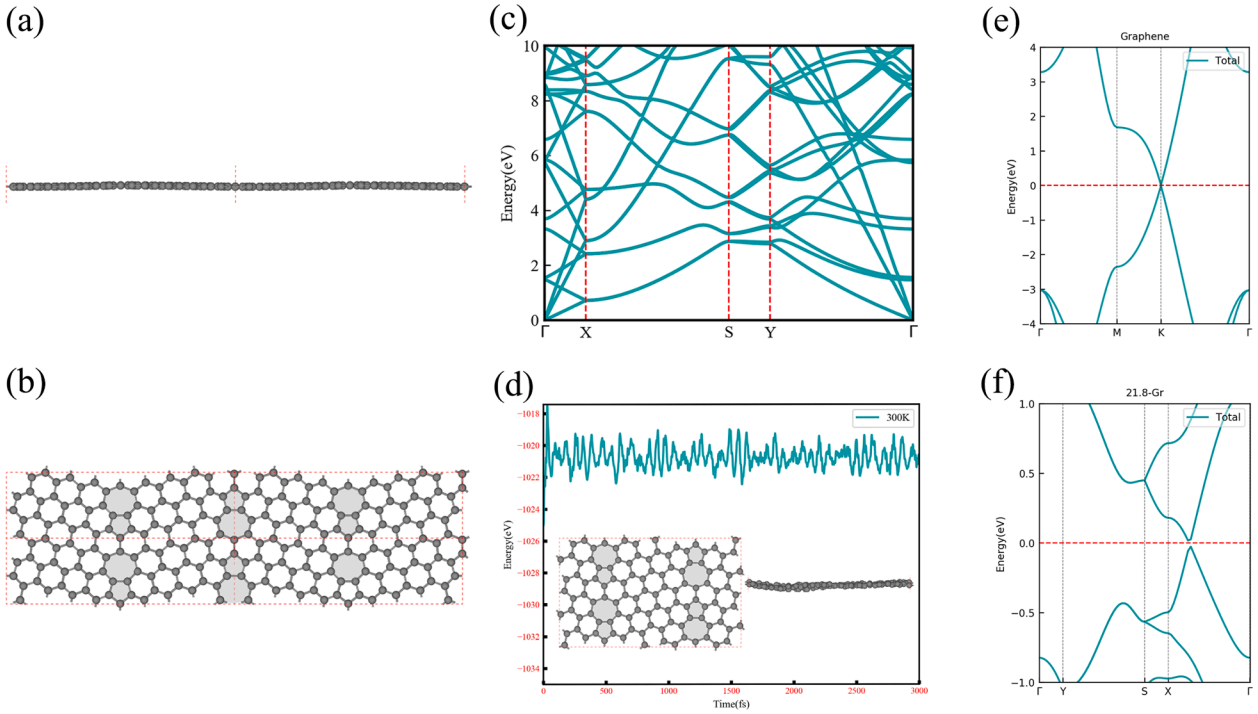

Fig. 1. (**a**) Top and (**b**) side view of the optimized model of 21.8-graphene. Red dashed boxes denote the supercell, grain boundaries are marked by shadows. **(c)** Phonon band structures and **(d)** Variation of the total potential energy of 21.8-Gr with simulation time during AIMD simulation at 300 K, respectively. The insets are the top and side views of the geometrical structures at the end of simulation. **(e)** and **(f)** denote the band structures of graphene and 21.8-graphene, respectively.

Ni are with one carbon atom on top of a metal atom, and the second carbon on a hollow site, namely top-fcc adsorption configuration, which are in consistent with previous studies [37–39].

The optimized structures of graphene with grain boundaries stacked on metal substrates are given in Fig. 2. With the introduction of grain boundaries, in the cases of Cu and Ni, on one side of the grain boundaries, the C-C pairs are arranged with top-fcc configuration. While on the other side of the grain boundaries, C-C pairs deviate from the top-fcc configuration due to the variation of the crystal orientation. We name these C-C pairs as non-top-fcc pairs, as shown in Fig. 2.

For the Cu case, the 21.8-graphene layer almost keeps flat and the grain boundaries sections slightly bend to the substrate, which makes the graphene layer closer to the Cu surface compared with CuGr contacts. The minimum distance between graphene and Cu surfaces is 3.069 Å for CuGr and 2.895 Å for 21.8-CuGr respectively, as listed in Table 1. However, with the increasing of metal-graphene interactions (for Pd and Ni cases), the morphology of graphene layer has been buckled. For the 21.8-PdGr, the grain boundaries are attracted by the Pd surfaces which makes the graphene layer exhibiting wave-like shape (Δh_{Gr} is 1.056 Å) and the d_{Gr-M} is significantly reduced from 2.853 Å in PdGr to 1.956 Å in 21.8-PdGr. For the Ni case, both the grain boundaries and the top-fcc pairs are attracted to Ni surface with minimum distance of 1.735 Å, while the non-top-fcc pairs present arch patterns and are repelled from the Ni surface.

In order to figure out why the grain boundaries parts are attracted by the metal surfaces, we analyzed the charge transfer between the interfaces based on Bader's method [40]. In Fig. 3**a** we displayed the histogram of the average charge transfer between carbon and metal atoms. In Cu and Pd cases, grain boundaries facilitate more electron transfers from metal slabs to graphene. For Ni case, on average, there are less charge transfer in 21.8-NiGr than in NiGr, however, more electron transfers occur for the top-fcc pairs (0.079e per C atom for 21.8-Ni| graphene and 0.059e for NiGr). In general, the grain boundaries in graphene will facilitate charge transfer in the graphene-metal contacts, which (as shown in Fig. 3**b**) strengthen the interaction between graphene and metal substrates in 21.8-MGr. And this conclusion is good consistent with the experimental result that pentagon–heptagon defects will enhance the interaction between graphene and metal [41].

Table 1
The Δh_{Gr}[Å] (global corrugation), d_{Gr-M}[Å] (defined as the minimum distance from graphene to metal surfaces), and binding energyE_{bin_vdW} (eV) of the commensurate MGr and 21.8-MGr contacts. Binding energy is defined as$E_{bin_vdW} = (E_{tot} - E_M - E_{Gr})/N_{Gr}$, E_{tot}, $E_M E_{tot}$ and $E_{Gr}$are the energies of MGr interfaces, metallic slab and graphene monolayer, respectively, and N_{Gr} is the number of the C-C pairs in graphene. A negative value for *E* indicates a binding system.

	CuGr	21.8-CuGr	PdGr	21.8-PdGr	NiGr	21.8-NiGr
Δh_{Gr} (Å)	0	0.146	0.015	1.057	0.006	1.201
d_{Gr-M} (Å)	3.069	2.895	2.853	1.956	2.071	1.735
E_{bin_vdW} (eV)	−0.185	−0.195	−0.253	−0.358	−0.356	−0.415

In Fig. 4 we display the differential charge density of the 21.8-MGr interfaces. For all these three cases, at the area where charge transfer occurs, p_z orbitals of the C atoms (C_{top}) directly above the metal atoms obtain some electrons, whereas σ orbitals of C_{top} atoms lose some electrons, which makes C_{top} atoms negatively charged (blue *iso*-surface). On the other hand, for the metal atoms below (M_{below}) the C_{top} atoms, differential charge density indicates charge reduction in d_{z^2} orbitals and accumulation in $d_{xz,yz}$ orbital.

To further understand the interaction of grain boundaries and metal slabs, in Fig. 5, we plotted the differential charge density around the

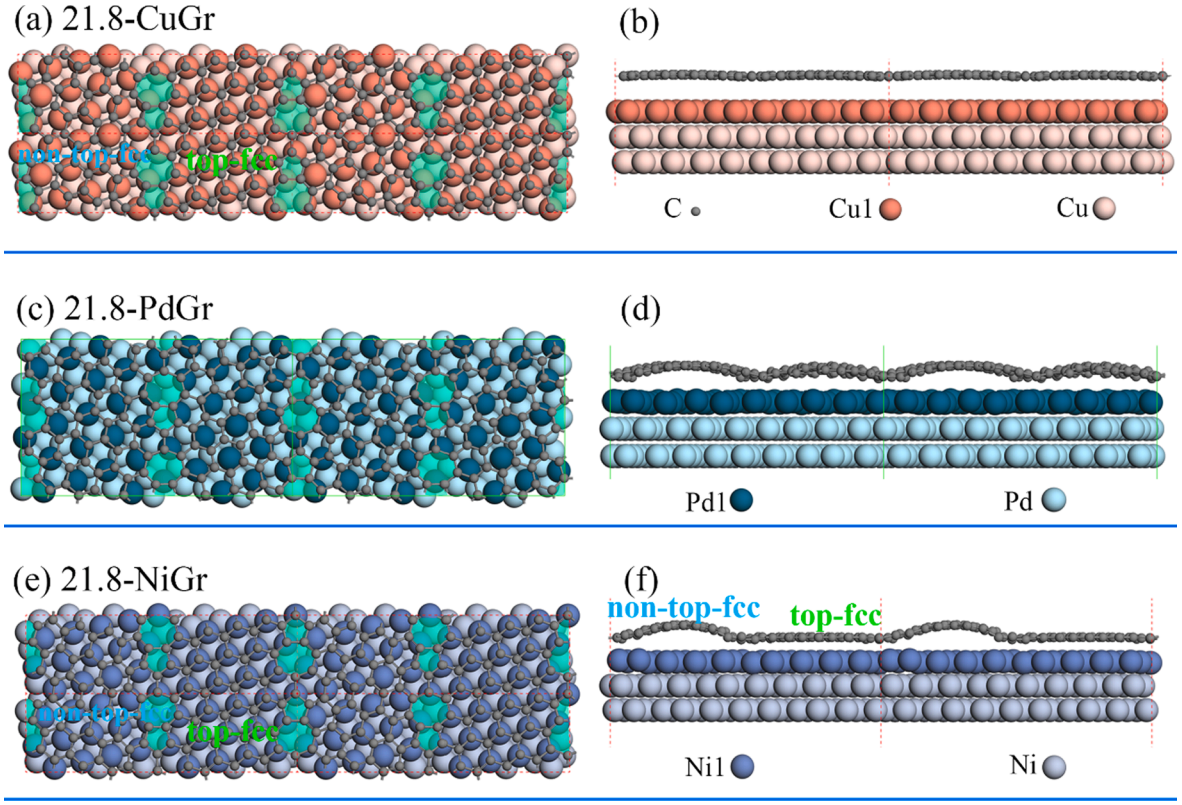

Fig. 2. (a) Top and (b) side view for optimized structure of 21.8-CuGr, (c) and (d) for 21.8-PdGr, (e) and (f) for 21.8-NiGr. The grain boundaries also marked by shadows. Red dashed boxes denote the supercells in Ni and Cu cases, while green boxes denote the supercells in Pd case. M1 means metal atoms in the first layer that is near the graphene layer.

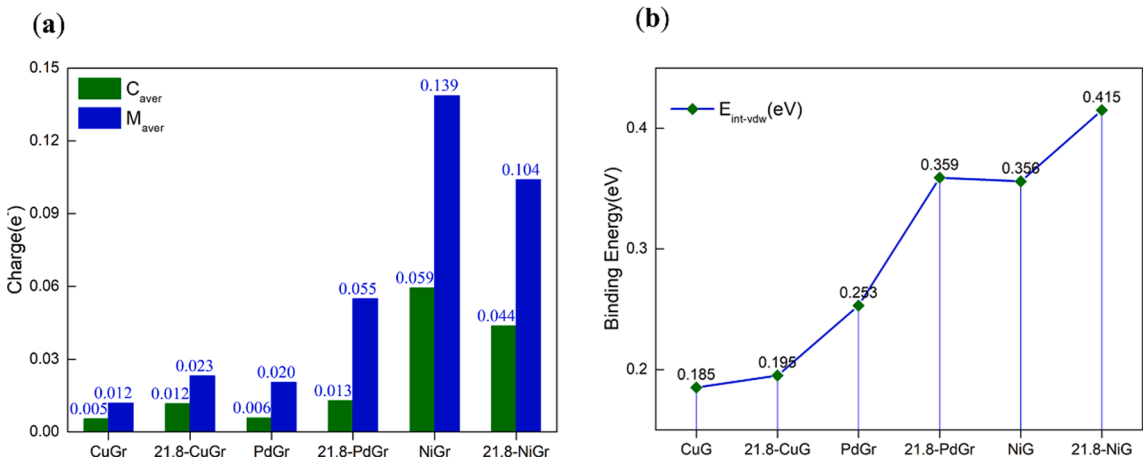

Fig. 3. **(a)** Bader analysis histogram and **(b)** Binding energy of the interfaces. Green color represents the average charges obtained by each carbon atom; blue color denotes the average charges lost by each metal atom in the metal layer close to graphene.

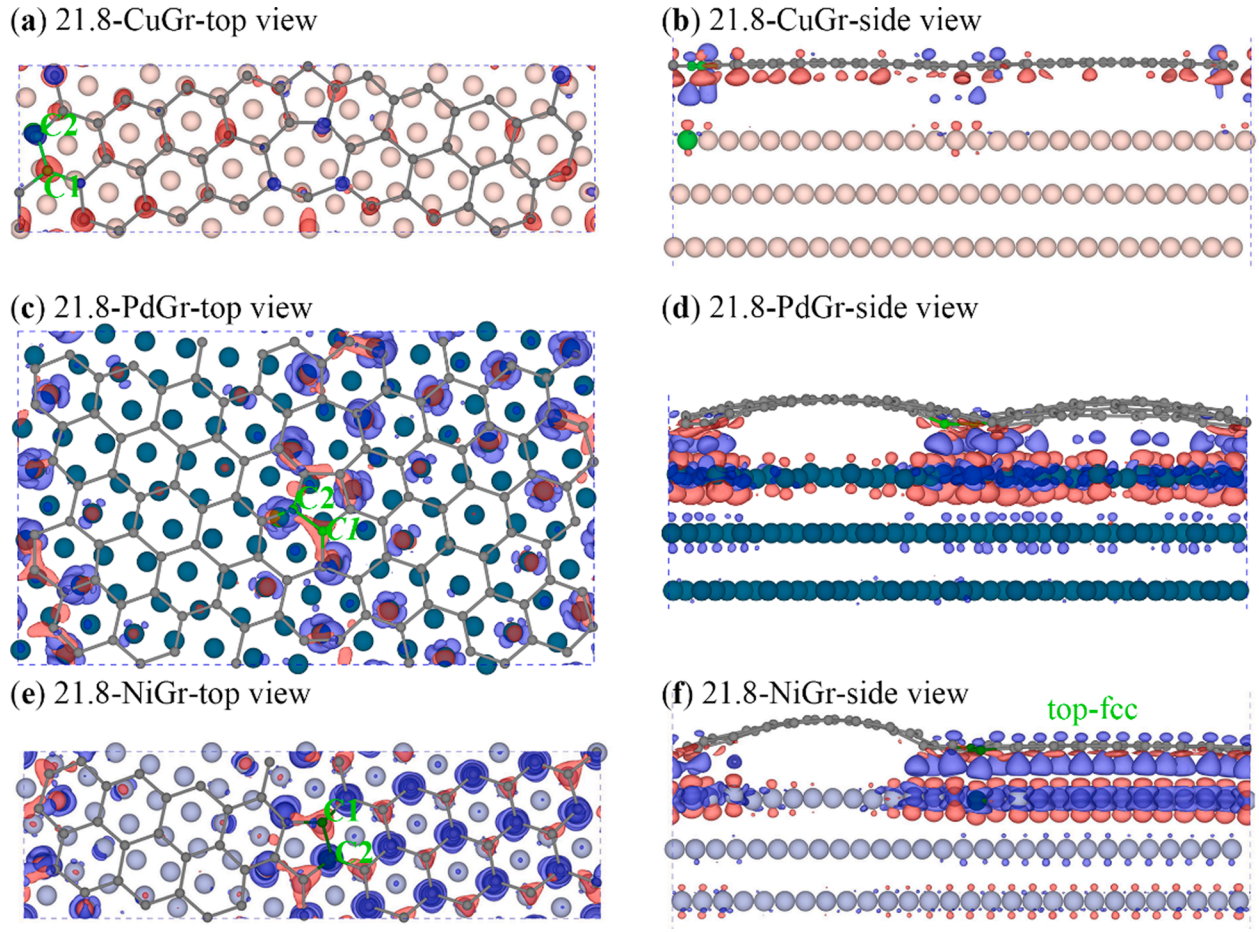

Fig. 4. Differential charge density with an *iso*-surface value of 0.0009 eÅ^{-3} for (a) top and (b) side view of 21.8-CuGr, 0.004 eÅ^{-3} for (c) top and (d) side view of 21.8-PdGr, and 0.0065 eÅ^{-3} for (e) top and (f) side view 21.8-NiGr, respectively. The blue and red regions indicate an increase and decrease in electron density, respectively.

local sections (across the C1, C2 and the metal atom below C2, and these three atoms are also marked by green color in Fig. 4). Obviously, in all three cases of Cu, Pd and Ni, C1 atoms donate electrons to C2 from their σ bonds, as a result, the p_z states of the C2 atoms in grain boundaries are further negatively charged compared to other C_{top} atoms. As a result, such interactions pin the monolayer graphene toward to metal surfaces.

For semiconductor and metal contacts, the charge injecting process involves the thermionic emission over the Schottky barrier and the tunneling emission across the barrier [42]. However, for graphene-metal contacts, the injection mainly depends on tunneling process, and the tunneling barrier should be low enough to enhance the transmission possibility of the carriers. A narrow and low tunneling barrier at the graphene-metal contacts can increase the electron injection. The height (Φ_{TB}) and width (W_{TB}) of tunneling barrier can be inferred from the

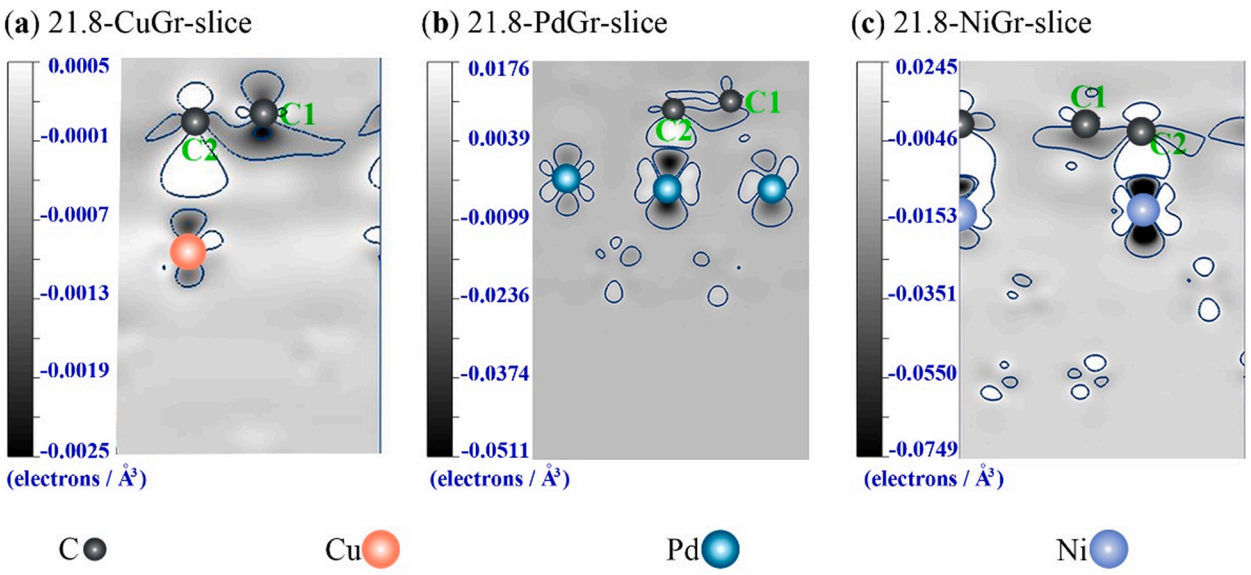

Fig. 5. Sectional map across the atoms marked by green colors in Fig. 4 of the differential charge density. (a) for 21.8-CuGr, (b) for 21.8-PdGr and (c) for 21.8-NiGr. The white and dark regions indicate an increase and decrease in electron density, respectively.

effective potential [43] at the MGr contact, which represents the carrier interaction with other electrons and the external electrostatic field [44]. As illustrated in Fig. 6, Φ_{TB} is the potential difference between vdW gap (Φ_{Gap}) and the Fermi level (E_F)of the structures, and w_{TB} is defined as the width of the square potential barrier.

The tunneling possibility (P_{TB}) is evaluated based on the equation [6,44,45]:

$$P_{\mathrm{TB}} = \exp\left(-\frac{2w_{\mathrm{TB}}}{\hbar}\sqrt{2m\Phi_{\mathrm{TB}}}\right)$$

where $\hbar$ is the reduced Planck's constant, m is the mass of the free electron, and w_{TB} and Φ_{TB}(shown in Fig. 6) is the width and height of the

Table 2
The calculated tunneling barrier width w_{TB}, height Φ_{TB} and tunneling probability P_{TB} of the with and without contacts.

	CuG	21.8-CuG	PdGr	21.8-PdGr	NiG	21.8-NiG
w_{TB}(Å)	1.339	1.205	1.110	0.536	0	0
Φ_{TB}(eV)	3.168	3.075	3.067	1.531	0	0
P_{TB}(%)	8.67	11.39	13.63	50.12	100	100

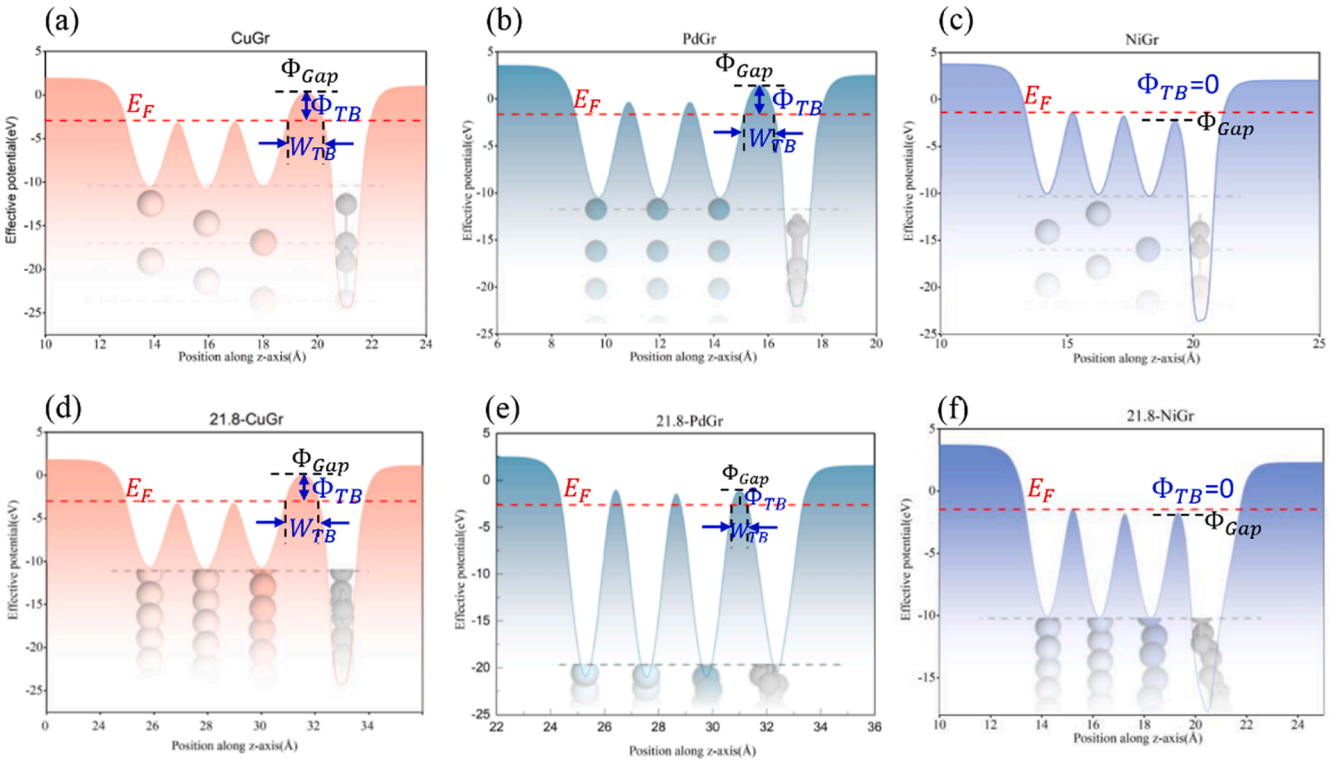

Fig. 6. Effective potential profile of (a) (b) and (c) for MGr, (d) (e) and (f) for 21.8-MGr. Red-dash line stands for Fermi level.

potential barrier. And the results of w_{TB}, Φ_{TB} and P_{TB} are also listed in Table 2.

As showed in Fig. 6**c and 6f**, for the Ni case, whether the contacts with or without GBs, due to the chemical bond formed between Gr and Ni, the tunneling probability is 100%, indicating high efficiency of carrier injection, this also confirms the experimental results [46] that the Ni contact has low resistance compares to other contacts [36]. For the Cu case, as shown in Fig. 6**a and 6d**, due to weak interaction, a very high and wide tunneling barrier formed between Cu and graphene monolayer, which indicates a very low efficiency of electron injection, leading to high contact resistance. However due to the appearance of grain boundaries, the tunneling possibility P_{TB} is improved from 8.67% in CuGr to 11.39% in 21.8-CuGr. Usually, strong interaction will lead to large tunneling probability, and for the Pd case, it has stronger interaction with graphene than Cu case which lead its larger probability (8.67% for CuGr and 13.63 for PdGr, as shown in Table 2), this general trend of our results is consistent with previous study [47]. And when grain boundaries appear in 21.8-PdGr, the width (height) of tunneling barrier is narrowed (lowered) from 1.110 to 0.536 Å (3.067 to 1.531 eV), and the tunneling possibility is largely increased from 13.63% to 50.12%. Thus, our results clearly indicate that the grain boundaries can increase the tunneling possibility of the graphene-metal contacts which further improve the performance of the graphene-based devices.

Generally, the grain boundaries are the undesirable components in intrinsic graphene layer which may degrade the electrical performance. However, Adam et al. [48] found that the electrical conductance is improved by one order of magnitude by GBs with better interdomain connectivity. Zhou et al. [49] also reported that graphene with boundary regions made up of dislocation exhibits relatively low resistivity which is comparable to the resistivity of the graphene sheet itself. Herein, based on our calculations, we also show that the contact resistance of the graphene-metal contact can be significantly decreased by the grain boundaries. It should be noted that considering the calculation resource, we only construct the grain boundaries with intermediate 5–7 ring pairs which has very low-density dislocations, however, we can easily experimentally synthesize the grain boundaries with continuous 5–7 or 4–8 rings and tune the distance between grain boundaries to increase the density of dislocations in graphene layer and thus further decrease the contact resistance. Therefore, our results suggest a very convenient strategy to control the performance of the contacts and provide new insight to design the graphene-based devices both theoretically and experimentally.

4. Summary

In this work we have presented a DFT study of graphene with grain boundaries layer and their contact with Cu, Pd and Ni(1 1 1) surfaces. Our results show that for graphene layer, the grain boundaries only induce small buckling and the band gap is opened about 45 meV. Due to the interlayer interactions, the grain boundaries areas of graphene are buckled toward the metal surfaces. For the strong interaction cases (Ni), due to the overlap of the orbits, the tunneling barrier is overcome completely. For the weak and intermediate interaction cases, grain boundaries can efficiently increase the tunneling possibility and thus decrease contact resistance. Thus, our results show that the grain boundaries can be an efficient method to control the contact performance of the graphene-based devices.

CRediT authorship contribution statement

Junfei Ding: Conceptualization, Methodology, Visualization, Writing - original draft, Writing - review & editing. **Qiushi Yao:** Resources, Investigation, Visualization. **Huasheng Sun:** Investigation. **Shanbao Chen:** Investigation. **Ting Hu:** Supervision, Writing - review & editing. **Erjun Kan:** Supervision, Resources, Funding acquisition, Writing - review & editing.

Declaration of Competing Interest

The authors declare that they have no known competing financial interests or personal relationships that could have appeared to influence the work reported in this paper.

Acknowledgements

The work is supported by the NSFC (11774173, 51790492, 51522206), the NSF of Jiangsu Province(BK20170831), and the Fundamental Research Funds for the Central Universities (No.30920021148, No.30915011203 and 30918011334). E. K. acknowledges the support from the Tianjing Supercomputer Centre and Shanghai Supercomputer Center.

Appendix A. Supplementary material

Supplementary data to this article can be found online at https://doi.org/10.1016/j.apsusc.2021.150392.

References

[1] A.K. Geim, I.V. Grigorieva, Van der Waals heterostructures, Nature 499 (2013) 419–425.
[2] D.L. Duong, S.J. Yun, Y.H. Lee, van der Waals Layered Materials: Opportunities and Challenges, ACS Nano 11 (2017) 11803–11830.
[3] T. Roy, M. Tosun, J.S. Kang, A.B. Sachid, S.B. Desai, M. Hettick, C.M.C. Hu, A. Javey, Field-Effect Transistors Built from All Two-Dimensional Material Components, Acs Nano 8 (2014) 6259–6264.
[4] K. Novoselov, A. Mishchenko, A. Carvalho, A.C. Neto, 2D materials and van der Waals heterostructures, Science 353 (2016) aac9439.
[5] D.S. Schulman, A.J. Arnold, S. Das, Contact engineering for 2D materials and devices, Chem. Soc. Rev. 47 (2018) 3037–3058.
[6] H. Jin, J.W. Li, L.H. Wan, Y. Dai, Y.D. Wei, H. Guo, Ohmic contact in monolayer InSe-metal interface, 2D Mater. 4 (2017) 8.
[7] R. Kappera, D. Voiry, S.E. Yalcin, B. Branch, G. Gupta, A.D. Mohite, M. Chhowalla, Phase-engineered low-resistance contacts for ultrathin MoS2 transistors, Nat. Mater. 13 (2014) 1128–1134.
[8] J.H. Kang, W. Liu, D. Sarkar, D. Jena, K. Banerjee, Computational Study of Metal Contacts to Monolayer Transition-Metal Dichalcogenide Semiconductors, Phys. Rev. X 4 (2014) 14.
[9] H. Liu, A.T. Neal, P.D. Ye, Channel Length Scaling of MoS2 MOSFETs, Acs Nano 6 (2012) 8563–8569.
[10] Y. Wen, P. He, Y.Y. Yao, Y. Zhang, R.Q. Cheng, L. Yin, N.N. Li, J. Li, J.J. Wang, Z. X. Wang, C.S. Liu, X. Fang, C. Jiang, Z.P. Wei, J. He, Bridging the van der Waals Interface for Advanced Optoelectronic Devices, Adv. Mater. 32 (2020) 7.
[11] C.J.L. de la Rosa, R. Phillipson, J. Teyssandier, J. Adisoejoso, Y. Balaji, C. Huyghebaert, I. Radu, M. Heyns, S. De Feyter, S. De Gendt, Molecular doping of MoS2 transistors by self-assembled oleylamine networks, Appl. Phys. Lett. 109 (2016) 4.
[12] L. Wang, I. Meric, P.Y. Huang, Q. Gao, Y. Gao, H. Tran, T. Taniguchi, K. Watanabe, L.M. Campos, D.A. Muller, J. Guo, P. Kim, J. Hone, K.L. Shepard, C.R. Dean, One-Dimensional Electrical Contact to a Two-Dimensional Material, Science 342 (2013) 614–617.
[13] C. Gong, D. Hinojos, W.C. Wang, N. Nijem, B. Shan, R.M. Wallace, K.J. Cho, Y. J. Chabal, Metal-Graphene-Metal Sandwich Contacts for Enhanced Interface Bonding and Work Function Control, Acs Nano 6 (2012) 5381–5387.
[14] Z. Yan, L. Ma, Y. Zhu, I. Lahiri, M.G. Hahm, Z. Liu, S. Yang, C. Xiang, W. Lu, Z. Peng, Z. Sun, C. Kittrell, J. Lou, W. Choi, P.M. Ajayan, J.M. Tour, Three-Dimensional Metal-Graphene-Nanotube Multifunctional Hybrid Materials, Acs Nano 7 (2013) 58–64.
[15] V. Mootheri, G. Arutchelvan, S. Banerjee, S. Sutar, A. Leonhardt, M.E. Boulon, C. Huyghebaert, M. Houssa, I. Asselberghs, I. Radu, M. Heyns, D. Lin, Graphene based Van der Waals contacts on MoS(2)field effect transistors, 2D Mater. 8 (2021) 10.
[16] X. Li, W. Cai, J. An, S. Kim, J. Nah, D. Yang, R. Piner, A. Velamakanni, I. Jung, E. Tutuc, Large-area synthesis of high-quality and uniform graphene films on copper foils, Science 324 (2009) 1312–1314.
[17] L. Gao, W. Ren, H. Xu, L. Jin, Z. Wang, T. Ma, L.-P. Ma, Z. Zhang, Q. Fu, L.-M. Peng, Repeated growth and bubbling transfer of graphene with millimetre-size single-crystal grains using platinum, Nat. Commun. 3 (2012) 699.
[18] P.A. Khomyakov, G. Giovannetti, P.C. Rusu, G. Brocks, J. van den Brink, P.J. Kelly, First-principles study of the interaction and charge transfer between graphene and metals, Phys. Rev. B 79 (2009).
[19] G. Giovannetti, P.A. Khomyakov, G. Brocks, V.M. Karpan, J. van den Brink, P. J. Kelly, Doping graphene with metal contacts, Phys. Rev. Lett. 101 (2008) 4.
[20] J. Wintterlin, M.L. Bocquet, Graphene on metal surfaces, Surface Sci. 603 (2009) 1841–1852.

[21] S.M. Kozlov, F. Viñes, A. Görling, Bonding Mechanisms of Graphene on Metal Surfaces, J. Phys. Chem. C 116 (2012) 7360–7366.
[22] J. Ding, D. Ahmed, H. Sun, S. Chen, Q. Yao, C. Huang, K. Deng, E. Kan, Hexagonal Boron Nitride-Metal Junction: Removing the Schottky Barriers by Grain Boundary, Adv. Theory Simulat. 1 (2018).
[23] J.M. Carlsson, L.M. Ghiringhelli, A. Fasolino, Theory and hierarchical calculations of the structure and energetics of [0001] tilt grain boundaries in graphene, Phys. Rev. B 84 (2011).
[24] K. Kim, Z. Lee, W. Regan, C. Kisielowski, M. Crommie, A. Zettl, Grain boundary mapping in polycrystalline graphene, ACS Nano 5 (2011) 2142–2146.
[25] P.Y. Huang, C.S. Ruiz-Vargas, A.M. van der Zande, W.S. Whitney, M.P. Levendorf, J.W. Kevek, S. Garg, J.S. Alden, C.J. Hustedt, Y. Zhu, Grains and grain boundaries in single-layer graphene atomic patchwork quilts, Nature 469 (2011) 389.
[26] J.P. Perdew, K. Burke, M. Ernzerhof, Generalized gradient approximation made simple, Physical Rev. Lett. 77 (1996) 3865.
[27] G. Kresse, J. Hafner, Ab initio molecular dynamics for liquid metals, Phys. Rev. B Condens. Matter 47 (1993) 558–561.
[28] S. Grimme, Semiempirical GGA-type density functional constructed with a long-range dispersion correction, J. Comput. Chem. 27 (2006) 1787–1799.
[29] V. Caciuc, N. Atodiresei, M. Callsen, P. Lazić, S. Blügel, Ab initio and semi-empirical van der Waals study of graphene–boron nitride interaction from a molecular point of view, Journal of Physics: Condensed Matter 24 (2012), 424214.
[30] S. Grimme, C. Mück-Lichtenfeld, J. Antony, Noncovalent interactions between graphene sheets and in multishell (hyper) fullerenes, The Journal of Physical Chemistry C 111 (2007) 11199–11207.
[31] G. Kresse, J. Furthmüller, Efficiency of ab-initio total energy calculations for metals and semiconductors using a plane-wave basis set, Computational Materials Science 6 (1996) 15–50.
[32] G. Kresse, J. Furthmüller, Efficient iterative schemes for ab initio total-energy calculations using a plane-wave basis set, Physical Review B 54 (1996) 11169.
[33] L. Bengtsson, Dipole correction for surface supercell calculations, Physical Review B 59 (1999) 12301.
[34] J. Neugebauer, M. Scheffler, Adsorbate-substrate and adsorbate-adsorbate interactions of Na and K adlayers on Al (111), Physical Review B 46 (1992) 16067.
[35] A. Togo, I. Tanaka, First principles phonon calculations in materials science, Scripta Materialia 108 (2015) 1–5.
[36] H.M. Liu, H. Kondo, T. Ohno, Contact effects of nickel and copper on electron transport through graphene, Physical Review B 86 (2012).
[37] T. Olsen, J. Yan, J.J. Mortensen, K.S. Thygesen, Dispersive and covalent interactions between graphene and metal surfaces from the random phase approximation, Phys Rev Lett 107 (2011), 156401.
[38] M. Vanin, J.J. Mortensen, A.K. Kelkkanen, J.M. Garcia-Lastra, K.S. Thygesen, K. W. Jacobsen, Graphene on metals: A van der Waals density functional study, Physical Review B 81 (2010).
[39] I. Hamada, M. Otani, Comparative van der Waals density-functional study of graphene on metal surfaces, Physical Review B 82 (2010).
[40] R.F. Bader, Atoms in molecules, Wiley Online, Library (1990).
[41] B.P. Klein, S.E. Harman, L. Ruppenthal, G.M. Ruehl, S.J. Hall, S.J. Carey, J. Herritsch, M. Schmid, R.J. Maurer, R. Tonner, C.T. Campbell, J.M. Gottfried, Enhanced Bonding of Pentagon-Heptagon Defects in Graphene to Metal Surfaces: Insights from the Adsorption of Azulene and Naphthalene to Pt(111), Chemistry of Materials 32 (2020) 1041–1053.
[42] A. Allain, J.H. Kang, K. Banerjee, A. Kis, Electrical contacts to two-dimensional semiconductors, Nature Materials 14 (2015) 1195–1205.
[43] A. Hassan, Y. Guo, Q. Wang, Y. Kawazoe, P. Jena, Interfacial properties of penta-graphene-metal contacts, J. Appl. Phys. 125 (2019).
[44] T. Shen, J.C. Ren, X.Y. Liu, S. Li, W. Liu, van der Waals Stacking Induced Transition from Schottky to Ohmic Contacts: 2D Metals on Multilayer InSe, Journal of the American Chemical Society 141 (2019) 3110–3115.
[45] E. Merzbacher, Quantum Mechanics, Willey, New York, 1998.
[46] K. Nagashio, T. Nishimura, K. Kita, A. Toriumi, Metal/graphene contact as a performance killer of ultra-high mobility graphene analysis of intrinsic mobility and contact resistance, in: 2009 IEEE International Electron Devices Meeting (IEDM), IEEE, 2009, pp. 1–4.
[47] T. Cusati, G. Fiori, A. Gahoi, V. Passi, M.C. Lemme, A. Fortunelli, G. Iannaccone, Electrical properties of graphenemetal contacts, Sci Rep 7 (2017) 11.
[48] A.W. Tsen, L. Brown, M.P. Levendorf, F. Ghahari, P.Y. Huang, R.W. Havener, C. S. Ruiz-Vargas, D.A. Muller, P. Kim, J. Park, Tailoring electrical transport across grain boundaries in polycrystalline graphene, Science 336 (2012) 1143–1146.
[49] X. Zhou, S.-H. Ji, S.P. Chockalingam, J.B. Hannon, R.M. Tromp, T.F. Heinz, A.N. Pasupathy, F.M. Ross, Electrical transport across grain boundaries in graphene monolayers on SiC(0 0 0 $\bar{1}$), 2D Mater. 5 (2018).